

Coherence Effects in Diffractive Electroproduction of ρ Mesons from Nuclei

T. Renk, G. Piller and W. Weise *

Physik Department
Technische Universität München
D-85747 Garching, Germany

Abstract

A systematic multiple scattering formalism for vector meson electroproduction from nuclei is developed, with emphasis on the formation, propagation and hadronization scales for quark-gluon fluctuations of the virtual high-energy photon. The theory is compared to HERMES measurements of ρ electroproduction on ^{14}N . The nuclear transparency as a function of the vector meson propagation length is well reproduced.

*) Work supported in part by BMBF and DFG.

1 Introduction

Electroproduction of vector mesons from nuclei is an excellent tool to investigate the formation and propagation of quark-antiquark pairs under well-controlled kinematical conditions. The observed nuclear coherence effects provide important information on properties of quark-gluon configurations present in the wave function of the interacting virtual photon, and on their hadronization into the finally observed vector meson. Recent data on ρ production from various nuclei have become available from measurements of the HERMES collaboration at DESY [1]. Earlier measurements at higher energies were performed at FNAL [2] and CERN [3].

Consider first the electroproduction of vector mesons from free nucleons. The four-momentum of the interacting virtual photon is denoted by $q^\mu = (\nu, \mathbf{q})$. We use $Q^2 = -q^2$, and $x = Q^2/2M\nu$ is the Bjorken scaling variable expressed in the lab frame, M is the nucleon mass. At large photon energies and small momentum transfers to the target nucleon, diffractive production mechanisms dominate: the vector meson emerges from the reaction leaving the nucleon intact.

According to the current understanding, the picture for this process is believed to be as follows: At $\nu \geq 3 \text{ GeV}$ and $x \leq 0.1$ one can decompose the amplitude for the diffractive production of a vector meson V in terms of colorless hadronic or quark-gluon fluctuations of the (virtual) photon (see e.g. [4, 5]):

$$f^{\gamma^* N \rightarrow VN} = \sum_h \frac{\langle 0 | \epsilon_{\gamma^*} \cdot J^{em} | h \rangle}{E_h - \nu} f^{hN \rightarrow VN}. \quad (1)$$

Here ϵ_{γ^*} is the polarization vector of the virtual photon, J^{em} denotes the electromagnetic current, and E_h stands for the energy of the intermediate hadronic state h .

At photon energies $3 < \nu < 30 \text{ GeV}$ and $Q^2 \lesssim 1 \text{ GeV}^2$, contributions to the photo-production amplitude $f^{\gamma^* N \rightarrow VN}$ from hadronic states with large invariant mass m_h are suppressed by large energy denominators $E_h - \nu \approx (m_h^2 + Q^2)/(2\nu)$. This restriction to light intermediate hadronic states implies vector meson dominance (see e.g. [6]): in the lab frame the photon converts into a vector meson prior to the scattering from the target.

On the other hand, at $Q^2 \gg 1 \text{ GeV}^2$ and $x \ll 0.1$ perturbative QCD is believed to be applicable [7]: in the lab frame the photon first converts to a quark-antiquark-gluon jet which then interacts with the nucleon. At high photon energies the finally observed vector meson is formed at a much later stage.

The transition from small to large Q^2 interpolates between non-perturbative hadron formation and perturbative quark-antiquark-gluon dynamics, a question of central importance in QCD. Nuclear targets are particularly helpful at this point because they serve as analyzers for the coherent interaction of the produced $q\bar{q}$ -gluon system with several nucleons [9]. The average distance between two nucleons provides the ‘‘femtometer scale’’

which can be used to measure the relevant coherence lengths (for reviews and references see [10, 11, 12]).

The production process is driven by the following characteristic scales. The propagation length (for reviews and references see e.g. [6, 13]),

$$\lambda \approx \frac{2\nu}{m^2 + Q^2}, \quad (2)$$

represents the longitudinal distance over which a hadronic fluctuation of invariant mass m propagates in the lab frame when induced by a photon of energy ν and virtuality Q^2 . At large Q^2 the initially produced wave packet is characterized by its transverse size b . For longitudinally polarized photons, detailed calculations suggest [8]

$$b = \frac{const}{Q}. \quad (3)$$

In perturbative QCD the minimal ($q\bar{q}$) Fock space component has $const \sim 4-5$ at $Q^2 \gtrsim 5 \text{ GeV}^2$ [14]. Thus for $Q^2 = 5 \text{ GeV}^2$ and $const = 4$, the transverse size of the initial wave packet is $b \simeq 0.35 \text{ fm}$, much smaller than the diameter of a fully developed ρ meson.

This paper is organized as follows. The multiple scattering theory for the vector meson electroproduction from nuclei, both coherent and incoherent, is developed in the next section. Section 3 presents results with detailed comparisons to the HERMES measurements, using ^{14}N targets, and a discussion of the observed transparency and propagation length effects. A concluding summary is given in Section 4.

2 Amplitudes and cross sections

In the following we derive amplitudes and cross sections for exclusive electroproduction of vector mesons from nuclei. Although we concentrate on ρ mesons, our formalism can be extended easily to other vector mesons.

At high energies the production of ρ mesons is driven by diffraction: the incident photon interacts with one of the nucleons in the nucleus and produces a hadronic state h , leaving the nucleon intact. The hadron h then propagates through the nuclear medium and possibly re-scatters, again diffractively, from further nucleons, subsequently forming the observed ρ meson.

The leading nuclear effects result from processes involving two nucleons as illustrated in Fig.1. The diffractive production of the intermediate hadronic state, $\gamma^* + N \rightarrow h + N$, is described by the amplitude f_{γ^*h} . At high energies this amplitude depends, to a good approximation, only on the momentum transfer \mathbf{k}_t perpendicular to the direction of the incoming photon. One introduces the profile function (see e.g. [6, 15]):

$$\Gamma_{\gamma^*h}(\mathbf{b}) = \frac{1}{2\pi i |\mathbf{q}|} \int d^2k_t f_{\gamma^*h}(\mathbf{k}_t) e^{i\mathbf{k}_t \cdot \mathbf{b}}, \quad (4)$$

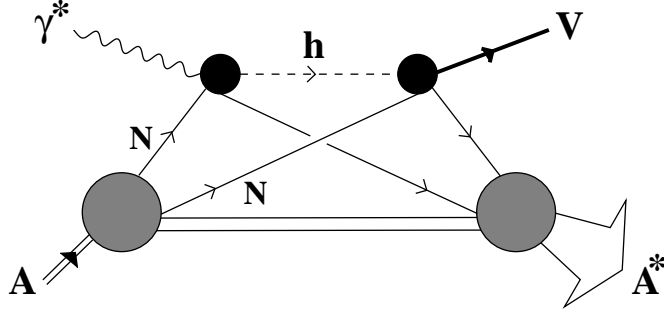


Figure 1: Double scattering contribution to (virtual) photoproduction of a vector meson.

where the three-momentum \mathbf{q} of the incident photon is chosen in the z -direction, $\mathbf{q} = \hat{z}|\mathbf{q}|$. $\Gamma_{\gamma^*h}(\mathbf{b})$ is a measure of the interaction strength at fixed impact parameter \mathbf{b} .

In the double scattering process illustrated in Fig. 1, the intermediate state h interacts with a second nucleon, producing the final ρ meson state, $h + N \rightarrow \rho + N$. The corresponding amplitude $f_{h\rho}$ defines a profile function $\Gamma_{h\rho}$ as in Eq.(4). In total, the double scattering contribution to ρ production is described by the nuclear profile operator

$$\Gamma_{\gamma^*\rho}^{A(2)}(\mathbf{b}, \mathbf{s}_i, \mathbf{s}_j) = \sum_{\{i \neq j\}=1}^A \Gamma_{h\rho}(\mathbf{b} - \mathbf{s}_j) e^{i\Delta_{h\rho}z_j} \theta(z_j - z_i) \Gamma_{\gamma^*h}(\mathbf{b} - \mathbf{s}_i) e^{i\Delta_{\gamma^*h}z_i}. \quad (5)$$

The two nucleons labeled i and j are located at impact parameters $\mathbf{b} - \mathbf{s}_{j,i}$ and at longitudinal distances $z_{i,j}$. The θ -function makes sure that the intermediate hadronic state h is produced before it re-scatters. The difference between the three-momenta of the incoming virtual photon and the hadronic state h with invariant mass m_h leads to the phase $e^{i\Delta_{\gamma^*h}z_i}$. For large photon energies ($\nu^2 \gg Q^2$ as well as $\nu \gg m_h$) transitions in the forward direction dominate, and one finds [6, 15]:

$$\Delta_{\gamma^*h} \approx \frac{Q^2 + m_h^2}{2\nu}, \quad (6)$$

which corresponds to the inverse of the longitudinal propagation length (2) of the intermediate system h . Similarly, the transition from the intermediate state h to the final ρ leads to the second phase in Eq.(5),

$$\Delta_{h\rho} \approx \frac{m_h^2 - m_\rho^2}{2\nu}. \quad (7)$$

This phase carries the information about the time it takes to form the final vector meson out of the intermediate state h . In fact $\Delta_{h\rho}$ is just the inverse of that formation time,

$$\tau_f = \frac{1}{\Delta_{h\rho}} \simeq \frac{\nu}{m_\rho \delta m} \quad (8)$$

with $\delta m = m_h - m_\rho$.

The role played by the phases (6,7) can be understood as follows: the nuclear scattering amplitude involves an integration of the nuclear profile operator over the volume of the target nucleus. The production process is dominated by contributions with phases roughly constant over the nuclear volume, while terms with rapidly oscillating phases are suppressed. This observation leads to the following scenarios depending on Q^2 :

- At large photon four-momenta ($Q^2 \gg 1 \text{ GeV}^2$) and small Bjorken- x ($x \ll 0.1$), the longitudinal interaction length $\lambda = \Delta_{\gamma^*h}^{-1}$ exceeds nuclear dimensions. Therefore, as seen from the lab frame, the photon first couples to a quark-antiquark pair which subsequently scatters from the nucleus. The $q\bar{q}$ pair has a chance to travel over large distances inside the nucleus and interacts only weakly, its cross section being proportional to $b^2 \sim 1/Q^2$. Since the formation time $\tau_f = \Delta_{h\rho}^{-1}$ is large in the considered kinematic region, the finally observed vector meson forms far outside the nucleus. This phenomenon is commonly referred to as color coherence or color (singlet) transparency [9, 10, 11, 12].
- At small photon virtualities, $Q^2 \lesssim 1 \text{ GeV}^2$, vector meson production is driven by the interaction of hadronic fluctuations of the photon. In particular the contribution of the ρ meson component in the photon spectral function dominates since it implies $\Delta_{h\rho} = 0$. At high energies, $\nu \sim 30 \text{ GeV}$, the ρ meson propagation length exceeds the size of the nucleus. Therefore, the photon first couples to low mass ($m_h \sim m_\rho$) hadronic states which then scatter from the nucleus. The interaction cross sections of these states are large, comparable to typical hadron-nucleon cross sections. As a consequence coherent multiple interactions with several nucleons lead to significant nuclear modifications of the production process.
- At $Q^2 \lesssim 1 \text{ GeV}^2$ and moderate energies, e.g. $\nu \sim 4 \text{ GeV}$, the longitudinal propagation length λ for a ρ meson is less than 1 fm, so that the meson is produced on a nucleon inside the nucleus. Once produced, the meson undergoes final state interactions with residual nucleons. Note however that the path of the vector meson through the nuclear medium is, on average, shorter than in the previous case, where hadronic states propagate through the nucleus as a whole. One therefore expects nuclear modifications of the ρ meson production cross section at low photon energies to be less pronounced than at high energies.

Higher order multiple scattering contributions involve transition amplitudes $f_{h'h}$ between different hadronic states carrying photon quantum numbers. These, as well as the complete set of amplitudes $f_{h\rho}$ which enter already in double scattering, Eq.(5), are in general unknown. Consequently, any calculation of vector meson production at high energies must involve some model assumptions about $f_{h'h}$ (for examples see [10, 11]). On the other hand, the recent HERMES data on exclusive ρ production were taken at moderate photon energies ν , where the typical formation times τ_f are less than, or at most of the order of, the average nucleon-nucleon separation in nuclei. Contributions to the produc-

tion process from intermediate ρ mesons are therefore supposed to dominate. They lead to the nuclear profile operator [6, 15]:

$$\Gamma_{\gamma^*\rho}^A(\mathbf{b}; \{\mathbf{s}\}) = \sum_{i=1}^A \left\{ \prod_{j \neq i} [1 - \Gamma_\rho(\mathbf{b} - \mathbf{s}_j) \theta(z_j - z_i)] \right\} \Gamma_{\gamma^*\rho}(\mathbf{b} - \mathbf{s}_i) \exp(i\Delta_{\gamma^*\rho} z_i), \quad (9)$$

which we use as a starting point for our investigations. Elastic ρ -nucleon scattering is described in Eq.(9) by the profile function $\Gamma_{\rho N \rightarrow \rho N} \equiv \Gamma_\rho$. Its relation to the ρN scattering amplitude $f_{\rho N \rightarrow \rho N} \equiv f_\rho$ is

$$\Gamma_\rho(\mathbf{b}) = \frac{1}{2\pi i |\mathbf{q}|} \int d^2 k_t f_\rho(\mathbf{k}_t) e^{i\mathbf{k}_t \cdot \mathbf{b}}. \quad (10)$$

2.1 Inclusive production

In the inclusive electroproduction of ρ mesons the nuclear final state is not observed. Summing over all possible nuclear excitations and applying closure leads to [6, 15]

$$\frac{d\sigma_{\gamma^*A \rightarrow \rho X}}{dt} = \frac{1}{4\pi} \int d^2 b \int d^2 b' e^{i\mathbf{k}_t \cdot (\mathbf{b}' - \mathbf{b})} \langle 0 | \Gamma_{\gamma^*\rho}^{A\dagger}(\mathbf{b}'; \{\mathbf{s}\}) \Gamma_{\gamma^*\rho}^A(\mathbf{b}; \{\mathbf{s}\}) | 0 \rangle. \quad (11)$$

Here $|0\rangle$ denotes the nuclear ground state; $t = (q - k)^2$ refers to the squared momentum transfer where k^μ is the four-momentum of the produced ρ meson.

The next step is to expand both nuclear profile operators in Eq.(11) in terms of nucleon profile functions, using Eq.(9). Collecting in $\Gamma_{\gamma^*\rho}^A$ and $\Gamma_{\gamma^*\rho}^{A\dagger}$ terms with products of at most n profile functions, Γ_ρ , defines the cross sections

$$\frac{d\sigma_{\gamma^*A \rightarrow \rho X}^{(n)}}{dt}. \quad (12)$$

They describe processes with up to $2n + 2$ nucleons involved in the production and re-scattering of the ρ -meson. At the high energies involved, it is justified to neglect NN -correlations and to treat the nucleus as a system of A independent nucleons, described by a density distribution $\rho_A(\mathbf{r})$. The cross sections in Eq.(12) are then expressed through nucleon amplitudes and nuclear form factors,

$$S_A(\mathbf{k}_t, \Delta) = \int d^2 b dz \rho_A(\mathbf{b}, z) e^{-i(\mathbf{k}_t \cdot \mathbf{b} + \Delta z)}. \quad (13)$$

In numerical calculations we use a Gaussian parametrization for the nuclear one-body density, applicable to light nuclei:

$$\rho_A(\mathbf{r}) = \left(\frac{3}{2\pi \langle r^2 \rangle_A} \right)^{3/2} \exp \left(-\frac{3r^2}{2 \langle r^2 \rangle_A} \right), \quad (14)$$

with normalization $\int d^3r \rho_A(\mathbf{r}) = 1$ and mean square radius $\langle r^2 \rangle_A = \int d^3r r^2 \rho_A(\mathbf{r})$.

The so-called single scattering contribution describes the production of a ρ meson through the interaction of the virtual photon with one nucleon inside the nucleus. Re-scattering from further nucleons does not occur here. One finds:

$$\frac{d\sigma_{\gamma^*A \rightarrow \rho X}^{(0)}}{dt} = A \frac{d\sigma_{\gamma^*N \rightarrow \rho N}}{dt} [1 + (A-1)S_A(\mathbf{k}_t, -\Delta_{\gamma^*\rho}) S_A(-\mathbf{k}_t, \Delta_{\gamma^*\rho})]. \quad (15)$$

The first term represents the A possibilities in which the nuclear profile operator and its conjugate in Eq.(11) involve the same nucleon. The second term counts $A(A-1)$ possibilities with Γ^A and $\Gamma^{A\dagger}$ involving different nucleons. This contribution is proportional to the square of the elastic nuclear form factor (13). As expected, the single scattering cross section reduces to A^2 times the exclusive ρ production cross section from free nucleons in the limit of vanishing momentum transfer ($\mathbf{k}_t, \Delta_{\gamma^*\rho} \rightarrow 0$).

The leading correction to single scattering results when one of the profile operators in Eq.(11) involves the re-scattering of the ρ meson from one nucleon in the target nucleus, while re-scattering terms are omitted in the second profile operator. We find

$$\begin{aligned} \frac{d\sigma_{\gamma^*A \rightarrow \rho X}^{(1)}}{dt} &= \frac{d\sigma_{\gamma^*A \rightarrow \rho X}^{(0)}}{dt} - \frac{A(A-1)}{2|\mathbf{q}|^3} \int d^2l \quad \text{Im} [f_{\gamma^*\rho}^*(\mathbf{k}_t) f_{\gamma^*\rho}(\mathbf{k}_t - \mathbf{l}) f_\rho(\mathbf{l})] \\ &\times \{S_A(\mathbf{l}, 0) S_A(-\mathbf{l}, 0) + S_A(-\mathbf{k}_t + \mathbf{l}, \Delta_{\gamma^*\rho}) S_A(\mathbf{k}_t - \mathbf{l}, -\Delta_{\gamma^*\rho}) \\ &\quad + (A-2) S_A(\mathbf{k}_t, -\Delta_{\gamma^*\rho}) S_A(-\mathbf{k}_t + \mathbf{l}, \Delta_{\gamma^*\rho}) S_A(-\mathbf{l}, 0)\} + \dots, \end{aligned} \quad (16)$$

where we have suppressed terms resulting from the square of re-scattering amplitudes. They can be found in the Appendix and are included in the numerical calculations.

At high energies the nucleon amplitudes $f_{\gamma^*\rho}$ and f_ρ are dominated by their imaginary parts. Re-scattering therefore reduces the production cross section, an observation first made in [4]. The first re-scattering term in Eq.(16) is proportional to $S_A(\mathbf{l}, 0) S_A(-\mathbf{l}, 0)$ and does not depend on the propagation length $\lambda = \Delta_{\gamma^*\rho}^{-1}$. This describes ρ production taking place on the same nucleon in both profile operators. The remaining contributions correspond to the interference of amplitudes where the ρ is produced on different nucleons. These terms are enhanced for large λ .

In our numerical calculations we have evaluated the inclusive production cross section (11) up to $n = 2$. This includes terms which account for the re-scattering of the produced ρ from up to 4 nucleons. Explicit expressions are given in the Appendix.

2.2 Coherent production

In coherent ρ production the target nucleus stays intact, i.e. one considers the reaction $\gamma^* + A \rightarrow \rho + A$, where the nucleus recoils as a whole and is left in its ground state. An experimental signature for this would be the detection of the recoiling nucleus. In practice

a situation like this is approximately realized at momentum transfers smaller than the nuclear Fermi momentum, $|t| < 0.1 \text{ GeV}^2$, where the nucleus responds quasi-elastically to the incoming virtual photon.

At high photon energies, the corresponding amplitude is related to the ground state matrix element of the nuclear profile function:

$$f_{\gamma^* A \rightarrow \rho A}(\mathbf{k}_t) = \frac{i|\mathbf{q}|}{2\pi} \int d^2b e^{-i\mathbf{k}_t \cdot \mathbf{b}} \langle 0 | \Gamma_{\gamma^* \rho}^A(\mathbf{b}; \{\mathbf{s}\}) | 0 \rangle. \quad (17)$$

As in the inclusive case, the ρ is produced in a diffractive interaction of the virtual photon with one of the nucleons in the nucleus, $\gamma^* + N \rightarrow \rho + N$. Then the ρ meson propagates through the residual nuclear system where it may interact with other nucleons. We expand the nuclear electroproduction amplitude (17) according to the number of ρ -nucleon re-scattering processes involved, following Eq.(9):

$$f_{\gamma^* A \rightarrow \rho A} = \sum_{n=0}^{A-1} f_{\gamma^* A \rightarrow \rho A}^{(n)}. \quad (18)$$

The amplitude $f_{\gamma^* A \rightarrow \rho A}^{(n)}$ includes all contributions to $f_{\gamma^* A \rightarrow \rho A}$ with products of n nucleon profile functions Γ_ρ or, equivalently, ρ -nucleon scattering amplitudes f_ρ . The cross sections

$$\frac{d\sigma_{\gamma^* A \rightarrow \rho A}^{(n)}}{dt} = \frac{\pi}{|\mathbf{q}|^2} \left| \sum_{i=0}^n f_{\gamma^* A \rightarrow \rho A}^{(i)}(\mathbf{k}_t) \right|^2. \quad (19)$$

describe the electroproduction of a ρ meson and its subsequent re-scattering from up to n nucleons.

The single scattering amplitude $f_{\gamma^* A \rightarrow \rho A}^{(0)}$ has no re-scattering. Within the independent particle description for the target nucleus one obtains:

$$f_{\gamma^* A \rightarrow \rho A}^{(0)}(\mathbf{k}_t) = A S_A(\mathbf{k}_t, -\Delta_{\gamma^* \rho}) f_{\gamma^* \rho}(\mathbf{k}_t). \quad (20)$$

The nuclear form factor in Eq.(20) accounts for the probability that the target nucleus stays intact during the interaction. S_A drops sharply for momenta much larger than the inverse nuclear radius, $|\mathbf{k}_t| > 1/R_A$, so that the single scattering contribution to coherent ρ production is small for $|t| > 1/R_A^2$.

If the produced ρ meson re-scatters from one nucleon after its production, one gets:

$$f_{\gamma^* A \rightarrow \rho A}^{(1)}(\mathbf{k}_t) = \frac{A(A-1)i}{4\pi|\mathbf{q}|} \int d^2l f_\rho(\mathbf{k}_t/2 + \mathbf{l}) f_{\gamma^* \rho}(\mathbf{k}_t/2 - \mathbf{l}) \times S_A(\mathbf{k}_t/2 + \mathbf{l}, 0) S_A(\mathbf{k}_t/2 - \mathbf{l}, \Delta_{\gamma^* \rho}). \quad (21)$$

The momentum transfer \mathbf{k}_t is now shared between the two nucleons participating in the interaction. This means that the form factors in Eq.(21) are probed, on average, at

lower momenta. This argument can be applied also to higher order multiple scattering amplitudes ($n > 1$) where the momentum transfer is shared between even more nucleons. Therefore, coherent ρ production from nuclei is most sensitive to multiple scattering processes when $|t|$ is large, a well known feature.

The scattering amplitude (17) has to be corrected for center-of-mass motion. This modification is important especially for light nuclei. For harmonic oscillator wave functions the c.m. correction can be calculated exactly [16]; it leads to an additional factor multiplying the coherent production amplitude (17):

$$f_{\gamma^*A \rightarrow \rho A}(\mathbf{k}_t) \rightarrow R_{recoil}(\mathbf{k}_t^2, \Delta) f_{\gamma^*A \rightarrow \rho A}(\mathbf{k}_t), \quad (22)$$

with

$$R_{recoil}(\mathbf{k}_t^2, \Delta) = \exp \left[\frac{(\mathbf{k}_t^2 + \Delta_\rho^2) \langle r^2 \rangle_A}{6A} \right]. \quad (23)$$

In numerical calculations we have evaluated the multiple scattering series (18) up to $n = 2$. The corresponding expressions are given in the Appendix.

2.3 Incoherent production

The incoherent ρ production cross section is obtained by taking the difference of the inclusive and coherent cross sections:

$$\frac{d\sigma_{incoh}^A}{dt} = \frac{d\sigma_{\gamma^*A \rightarrow \rho X}}{dt} - \frac{d\sigma_{\gamma^*A \rightarrow \rho A}}{dt}. \quad (24)$$

Multiple scattering contributions are defined via Eqs.(12,19):

$$\frac{d\sigma_{incoh}^{A(n)}}{dt} = \frac{d\sigma_{\gamma^*A \rightarrow \rho X}^{(n)}}{dt} - \frac{d\sigma_{\gamma^*A \rightarrow \rho A}^{(n)}}{dt}. \quad (25)$$

In the absence of re-scattering, i.e. for single scattering, one finds from Eqs.(15,20):

$$\frac{d\sigma_{incoh}^{A(0)}}{dt} = A \frac{d\sigma_{\gamma^*N \rightarrow \rho N}}{dt} [1 - S_A(\mathbf{k}_t, \Delta_{\gamma^* \rho})^2 + A S_A(\mathbf{k}_t, \Delta_{\gamma^* \rho})^2 (1 - R_{recoil}^2(\mathbf{k}_t^2, \Delta))]. \quad (26)$$

We observe that, even in the absence of re-scattering, the incoherent ρ production cross section from a nucleus does not reduce to the production cross section from a single nucleon times the number of nucleons inside the target nucleus. The interference of production processes occurring on different nucleons (see discussion in Section 2.1), as well as nuclear recoil, leads to a reduction of the nuclear cross section. Nevertheless, for heavy nuclei and/or large momentum transfers the nuclear form factors in Eq.(26) are small and one obtains approximately $d\sigma_{incoh}^{A(0)}/dt \approx A d\sigma_{\gamma^*N \rightarrow \rho N}/dt$.

In our numerical studies we calculate the multiple scattering contributions up to $n = 2$. A discussion of their properties and a comparison with data from HERMES follows in Section 3.

2.4 Vector meson dominance

The recent HERMES data on incoherent ρ production from nuclei were taken in the kinematic range $0.4 \text{ GeV}^2 < Q^2 < 5 \text{ GeV}^2$ and $9 \text{ GeV} < \nu < 20 \text{ GeV}$. At these moderate photon energies the observed nuclear effects should be caused primarily by the coherent multiple scattering of the ρ meson with several nucleons (see the discussion in Section 2). It is therefore justified to model the ρ -nucleon scattering amplitude, f_ρ , using Vector Meson Dominance (VMD).

We also employ VMD to describe the (virtual) photoproduction of the ρ meson from individual nucleons. Assuming VMD to be valid, the ρ production amplitude is related to the scattering amplitude by a kinematic prefactor. When discussing nuclear phenomena in terms of transparency ratios, i.e. the ratios of nuclear and free nucleon production cross sections, details of the VMD photoproduction amplitude cancel, in particular those parts which would give an inadequate description at $Q^2 > 1 \text{ GeV}^2$.

VMD relates the virtual photoproduction amplitude $f_{\gamma^*\rho}$ and the elastic ρ -nucleon scattering amplitude f_ρ [6]. For transversely polarized photons one has:

$$f_{\gamma_T^*\rho} = \frac{\sqrt{\alpha_{em}\pi}}{g_\rho} \frac{m_\rho^2}{m_\rho^2 + Q^2} f_\rho, \quad (27)$$

with the electromagnetic coupling constant $\alpha_{em} = 1/137$, the ρ meson mass $m_\rho = 0.77 \text{ GeV}$, and the coupling constant $g_\rho = 5.0$. The production amplitude for longitudinally polarized photons is given by:

$$f_{\gamma_L^*\rho} = \xi \frac{\sqrt{Q^2}}{m_\rho} f_{\gamma_T^*\rho}, \quad (28)$$

where $\xi \approx 0.7$ is the ratio of the elastic longitudinal and transverse vector meson-nucleon scattering amplitudes (see e.g. [17]). It remains to fix the amplitude f_ρ . We use the parametrization:

$$f_\rho(\mathbf{k}_t) = \frac{|\mathbf{q}|}{4\pi} \sigma_{\rho N} (i + \beta) e^{-B\mathbf{k}_t^2}, \quad (29)$$

with the total ρ -nucleon scattering cross section $\sigma_{\rho N}$, the ratio of the real to imaginary parts of the scattering amplitude, β , and the slope parameter B .

For the photoproduction amplitudes (27,28) we use empirical parameters which will be discussed in the following section.

Since the ratio of longitudinally to transversely polarized photons is determined by the kinematics of the process (see e.g. [6]) we have now everything prepared to calculate nuclear production cross sections.

While it is not the aim to calculate polarized cross sections in this work, we do note that polarization is an important observable against which models can be tested (see e.g. [22, 23]).

2.5 Discussion

Before presenting results we discuss points at which our present calculation differs from previous calculations. The standard treatment of vector meson electroproduction from nuclei within the framework of VMD and Glauber multiple scattering theory is summarized in Refs.[6, 15, 19, 20]. Several simplifying but not always justified approximations are commonly made. It is usually assumed that all momentum is transferred to the target nucleus during the production of the vector meson from one of the nucleons. After that the propagation of the vector meson through the nuclear medium is taken in forward direction. However, in a treatment of the multiple scattering series in Eq.(9) without further simplifying assumptions, as carried out here, one naturally encounters contributions to the production process with the momentum transfer *shared* between all participating nucleons. These contributions, which are usually neglected, become increasingly important with rising $|t|$.

A further approximation common to most treatments of coherent vector meson production is the exponentiation of the multiple scattering series. While this is a reasonable approximation for heavy nuclei, it should not be used for light ones.

In the incoherent case it is usually assumed that the vector meson is produced on one specific nucleon. Interferences of production processes which occur on different nucleons are omitted, so that contributions proportional to nuclear form factors (see e.g. (15)) are absent. Exponentiation of the multiple scattering series is frequently done also for the case of incoherent vector meson production. This approximation ignores contributions in which the momentum transfer is shared between several interacting nucleons.

So far, only total production cross sections have been measured with admittedly large experimental uncertainties [1, 2] so that the simplifying approximations, used e.g. in Ref.[20], are not very harmful. However, as soon as one wants to describe differential cross sections in a more quantitative way a complete term-by-term treatment of multiple scattering processes, as done here, is necessary since the $|t|$ -dependence of the cross section is greatly influenced by re-scattering processes.

3 Results

In the actual calculation we have to fix the free parameters of the ρ -nucleon scattering amplitude, f_ρ Eq. (29). For the total cross section we use $\sigma_{\rho N} = 25$ mb in the kinematic range of the HERMES experiment [6]. We have varied $\sigma_{\rho N}$ in the range between 22 mb and 30 mb, however these variations do not lead to dramatic changes in the results when considering ratios. The ratio of real to imaginary part of the amplitude was fixed at $\xi = -0.2$.

It remains to fix the slope parameter B both for production and re-scattering. In the case

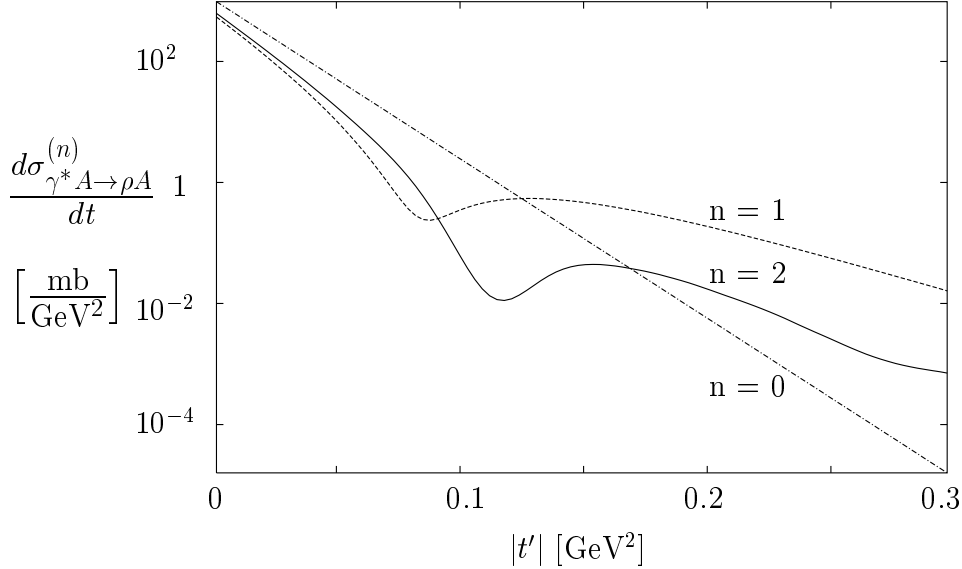


Figure 2: Differential cross section for coherent ρ production, $\gamma^*A \rightarrow \rho A$, on ^{14}N at $\nu = 14$ GeV and $Q^2 = 0.5$ GeV 2 , plotted against $|t'| = |t - t_0|$ (see text). Multiple scattering contributions with up to $n = 2$ are shown stepwise.

of production, several measurements of the diffractive slope can be found in the literature ([24, 25, 26, 27, 28, 29, 30]). A general tendency of decreasing slope with increasing Q^2 is observed, however the data are not precise enough to extract the slope unambiguously. We use the ansatz $B(Q^2) = \frac{1}{3} (r_N^2 + r_{q\bar{q}}^2(Q^2))$ which relates B to the radius of the target nucleon and the Q^2 -dependent size of the $q\bar{q}$ Fock state of the interacting photon, where $r_{q\bar{q}}^2 = a/(b + Q^2)$ meets the predictions of perturbative QCD for large Q^2 . We require this to agree with the HERMES result within the kinematic range of the experiment and use $B(Q^2 = 1 \text{ GeV}^2) \approx 8 \text{ GeV}^{-2}$ and $B(Q^2 = 5 \text{ GeV}^2) \approx 6 \text{ GeV}^{-2}$. A fit fixes the constants $a = 89.9$ and $b = 5.9 \text{ GeV}^2$.

For the diffractive slope of the re-scattering process we use a constant slope parameter $B_\rho = 8 \text{ GeV}^{-2}$ which is appropriate for the HERMES kinematics and is chosen in such a way that the incoherent slope, after taking re-scattering modifications into account, agrees best with the data.

Before confronting our calculations with data we summarize general features of vector meson production cross sections from nuclei. Typical results for coherent and incoherent ρ production from ^{14}N are shown in Figs.2 and 3. The energy and virtuality of the interacting photon has been fixed at $\nu = 14$ GeV and $Q^2 = 0.5 \text{ GeV}^2$, a kinematic range where VMD is applicable.

In Fig.2 we show the multiple scattering cross sections $d\sigma_{\gamma^*A \rightarrow \rho A}^{(n)}/dt$ from Eq.(19) for

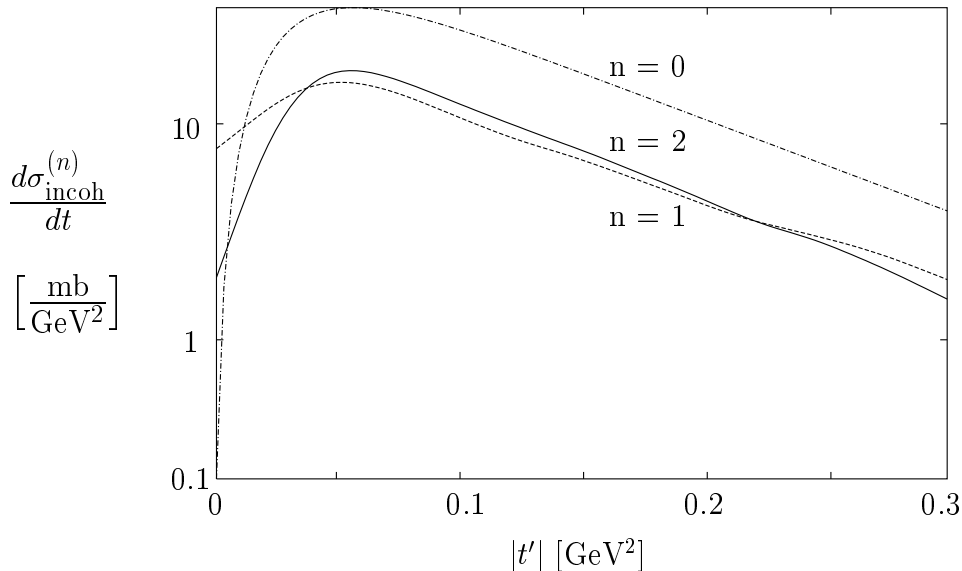


Figure 3: Differential cross section for incoherent ρ production, $\gamma^*A \rightarrow \rho X$, on ^{14}N at $\nu = 14$ GeV and $Q^2 = 0.5$ GeV 2 , plotted versus $|t'| = |t - t_0|$. Multiple scattering contributions with up to $n = 2$ are shown separately.

coherent ρ production plotted against $t' = t - t_0$, with the threshold momentum transfer $t_0 \simeq -[(Q^2 + m_\rho^2)/2\nu]^2$. We observe that the production cross section is strongly peaked at small $|t| < 0.05$ GeV 2 where single scattering dominates. This behavior is controlled by the nuclear form factor present in the single scattering amplitude (20). For Gaussian densities one finds $d\sigma^{(0)}/dt \sim S_A^2 \sim e^{-B_A|t|}$ with $B_A = \langle r^2 \rangle_A/3$. In the case of ^{14}N one has $\langle r^2 \rangle_A^{1/2} = 2.6$ fm [21], leading to $B_A \simeq 57$ GeV $^{-2}$.

With increasing $|t|$ multiple scattering gains in importance. At $0.05 \text{ GeV}^2 < |t| < 0.15 \text{ GeV}^2$ the interference between single and double scattering leads to a significant reduction of the production cross section. For larger values of $|t|$ multiple scattering adds substantially to the single scattering cross section and eventually dominates.

Incoherent ρ production cross sections $d\sigma_{incoh}^{A(n)}/dt$ from Eq.(25) are shown in Fig.3. One finds a much weaker dependence on the momentum transfer $|t|$ as compared to the coherent case. An investigation of single and multiple scattering contributions from Section 2.1 shows that the t -dependence is governed here by the behavior of the virtual photon-nucleon and ρ -nucleon scattering cross sections. These are, in a first approximation, proportional to $e^{-B|t|}$ with $B \simeq 7$ GeV $^{-2}$. Finally, a comparison of single and multiple scattering cross sections shows that single scattering dominates the incoherent production cross section for $|t| < 0.5$ GeV 2 . In this region multiple scattering reduces the cross section.

In summary: coherent vector meson production from nuclei at $|t| > 1/\langle r^2 \rangle_A$ provides an optimal window for an investigation of coherence phenomena. In this region the cross section is most sensitive to multiple scattering. However, the coherent production cross section is already quite small here – several orders of magnitude smaller than the incoherent one at large $|t|$.

3.1 Exclusive ρ production at HERMES

The HERMES collaboration has recently produced data [1] on exclusive electroproduction of ρ mesons from protons, deuterium, ^3He , and ^{14}N . The range of energy and momentum transfer available in this experiment is $9 \text{ GeV} < \nu < 20 \text{ GeV}$ and $0.4 \text{ GeV}^2 < Q^2 < 5 \text{ GeV}^2$. This implies coherence lengths for ρ mesons,

$$\lambda_\rho = \frac{2\nu}{m_\rho^2 + Q^2}, \quad (30)$$

in the range $0.6 \text{ fm} < \lambda < 8 \text{ fm}$ covering scales from the size of individual nucleons up to and beyond nuclear dimensions.

3.1.1 Cross sections

In Fig.4 the rate of produced ρ 's is plotted for ^3He and ^{14}N against t . At $|t'| = |t-t_0| \ll 0.1 \text{ GeV}^2$ coherent production dominates, leaving the nucleus as a whole in the ground state. Such coherent processes fall off rapidly with the nuclear form factor, so that at $|t'| \gtrsim 0.1 \text{ GeV}^2$ mostly incoherent ρ production from individual nucleons remains.

The result of our calculation, as discussed in Section 2.1, is shown for comparison. We include contributions to the inclusive production cross section (11) up to $n = 2$, accounting for the re-scattering from up to 4 nucleons. Since no explicit normalization of the data is given in Ref.[1], the normalizations of the calculated ^3He and ^{14}N cross sections have been adjusted to the data in the lowest $|t|$ -bin. The r.m.s. radii used in these calculations are $\langle r^2 \rangle_{^{14}\text{N}}^{1/2} = 2.6 \text{ fm}$ and $\langle r^2 \rangle_{^3\text{He}}^{1/2} = 1.9 \text{ fm}$ [21]. Good agreement with the observed t -dependence is found.

We also show our result for coherent ρ production. As expected, at small $|t|$ coherent production dominates the inclusive cross section, whereas it drops very rapidly with rising $|t|$.

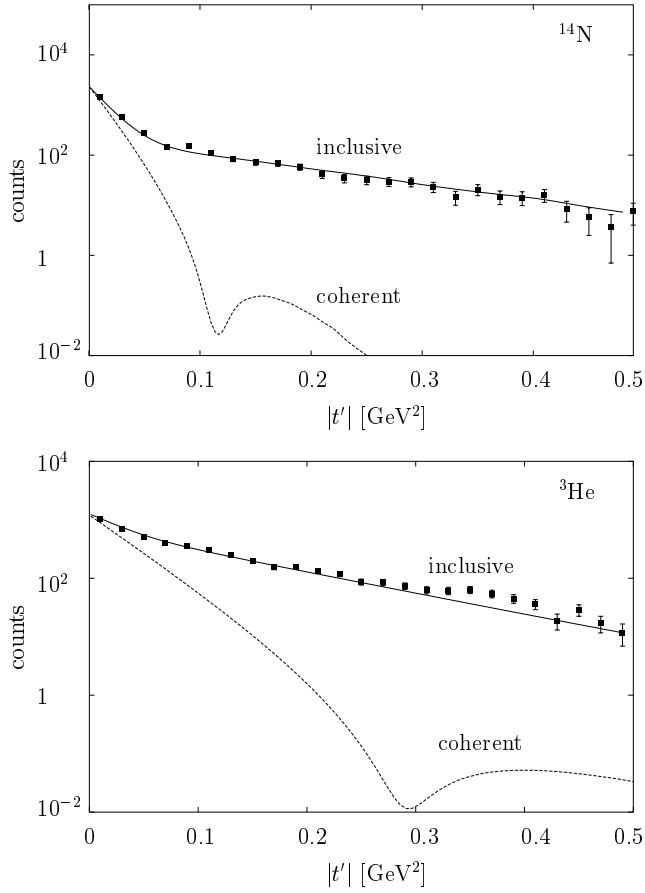


Figure 4: Diffractive ρ production from ^{14}N and ^3He . The data are from the HERMES collaboration [1]. The full (dashed) curves show our results for inclusive (coherent) ρ production.

3.1.2 Transparency

The HERMES collaboration has focused on nuclear effects in incoherent ρ production. For this purpose the transparency ratio

$$T_A = \frac{\sigma_{incoh}^A}{A \sigma_{\gamma^* N \rightarrow \rho N}}, \quad (31)$$

has been analyzed as a function of the ρ meson propagation length λ_ρ from Eq.(30). The total incoherent ρ production cross section in Eq.(31) is denoted by $\sigma_{incoh}^A = \int_{-\infty}^0 dt d\sigma_{incoh}^A/dt$, and $\sigma_{\gamma^* N \rightarrow \rho N}$ is the total diffractive ρ production cross section from

free nucleons. In the absence of re-scattering processes one obtains from Eqs.(15,20):

$$T_A^{(0)} = 1 - \frac{1}{\sigma_{\gamma^* N \rightarrow \rho N}} \int_{-\infty}^0 dt \frac{d\sigma_{\gamma^* N \rightarrow \rho N}}{dt} S_A(\mathbf{k}_t, \Delta_{\gamma^* \rho})^2 [1 - A(1 - R_{recoil}^2(\mathbf{k}_t^2, \Delta_{\gamma^* \rho}))]. \quad (32)$$

Incoherent ρ production from A nucleons gives $T_A^{(0)} = 1$. A reduction of $T_A^{(0)}$ is caused by the second term in Eq.(32) which results from nuclear recoil and the interference of production amplitudes involving different nucleons.

Starting out from the measured inclusive events (Fig. 4) the HERMES collaboration has constructed a data sample which approximately represents incoherent ρ production according to the following procedure: coherent ρ production processes have been approximated by an exponential form ($\sim e^{-|t|B}$) fitted to the inclusive data at small $|t|$. This contribution has then been subtracted from the inclusive events. The result so obtained has been used as incoherent data sample for momentum transfers $|t'_{\lambda_\rho}| < |t| < 0.4 \text{ GeV}^2$. The lower limit t'_{λ_ρ} varies for different bins of the ρ meson propagation length. It is chosen such that the exponential fit to the small $|t|$ data amounts to less than 5% of all inclusive events.

The measured transparency ratio T_A for ^{14}N is plotted in Fig.5. The deviation from unity at $\lambda_\rho \lesssim 1 \text{ fm}$ comes mainly from the final state re-scattering of the ρ meson after being produced on one of the nucleons. With increasing propagation length λ_ρ the transparency ratio decreases systematically. Hadronic fluctuations of the photon can scatter coherently on several nucleons also prior to the production of the final state vector meson, leading to an enhancement of nuclear effects.

In Fig.5 we present results of our calculation within the framework of VMD, using HERMES values for the average Q^2 and ν for each data bin. The full curve shows our result, adapting the HERMES construction of incoherent events: starting out from the calculated inclusive cross section we subtract an exponential fit to the low- $|t|$ result, and use the HERMES thresholds t'_{λ_ρ} as described previously. We find good agreement with the data. This suggests that the propagation of initially produced quark-gluon or hadronic states through the nuclear environment is dominated by contributions which interact about as strongly as the produced ρ meson. For comparison we also present results for the incoherent transparency ratio as obtained from the difference of the calculated inclusive and coherent cross sections. The deviation from the previous result points at ambiguities in the HERMES definition of incoherent events.

Let us have a closer look at the kinematics involved in the HERMES experiment. Large propagation length, $\lambda_\rho > 2 \text{ fm}$, corresponds to data taken at high energy transfers ν accompanied by small Q^2 . This is the VMD situation in which the photon predominantly converts into a ρ meson which then experiences coherent multiple scattering. For small propagation lengths, $\lambda_\rho < 2 \text{ fm}$, data were taken at average values \bar{Q}^2 between 2.5 and 5 GeV^2 and $\bar{\nu} \simeq 12 \text{ GeV}$. At such large Q^2 , quark-gluon degrees of freedom should already be relevant in the initial interaction of the virtual photon with one of the nucleons in the

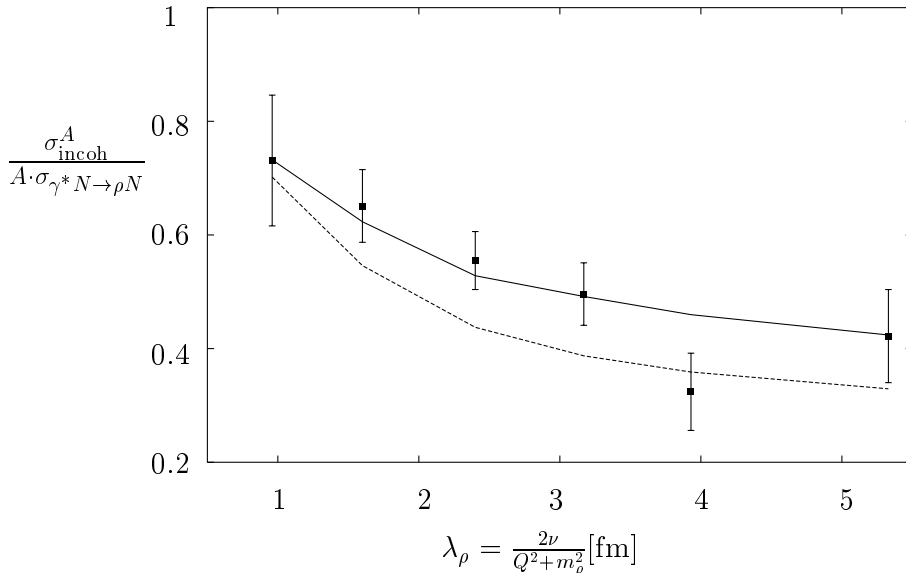


Figure 5: The transparency ratio T_A from Eq.(31) for ^{14}N . The data are from the HERMES collaboration [1]. The full curve shows the result of our calculation which has been adapted to the HERMES definition of incoherent events. The dashed curve shows the transparency ratio as obtained from the difference of the calculated inclusive and coherent cross section.

target nucleus. Perturbative QCD calculations [14] show indeed that, for longitudinally polarized photons with $Q^2 \simeq 5 \text{ GeV}^2$, the transverse size of the initially produced quark-antiquark wave packet is only a small fraction of the diameter of a fully developed ρ meson. Still, the time τ_f to form a ρ meson out of the primary $q\bar{q}$ wave packet under these conditions is small. Let the invariant mass of the wave packet be of order \bar{Q} . Using Eqs.(8,7) we estimate $\tau_f \sim 2\bar{\nu}/(\bar{Q}^2 - m_\rho^2) < 2.5 \text{ fm}/c$ for $\bar{Q} > 2.5 \text{ GeV}^2$ and $\bar{\nu} \simeq 12 \text{ GeV}$. Thus the $q\bar{q}$ pair is quite likely to be a ρ meson by the time it has crossed the average distance between two nucleons in ^{14}N , and its multiple scattering is then governed by the large ρN (rather than the small color-dipole) cross section. This is consistent with our observation that the VMD description of the measured propagation length effects works well over the full kinematic range of the HERMES data.

3.2 Aspects of color singlet transparency

Nuclear effects in incoherent ρ production as observed by the HERMES collaboration result from the coherent re-scattering of hadronic components present in the photon spectral function. On the other hand, at $Q^2 \gg 1 \text{ GeV}^2$ small sized quark-gluon wave packets are produced in photon-nucleon collisions. Their color dipole moment or, equivalently,

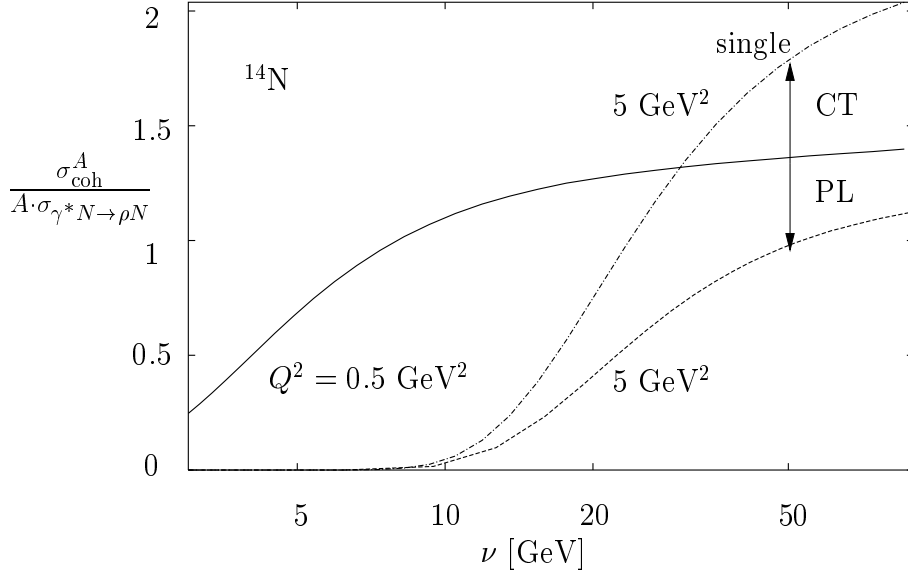


Figure 6: The transparency ratio for coherent ρ production from ^{14}N . The full (dashed) curve corresponds to the VMD calculation at $Q^2 = 0.5 \text{ GeV}^2$ (5 GeV^2). The dash-dotted curve shows the single scattering result for $Q^2 = 5 \text{ GeV}^2$. The arrows indicate the behavior of the transparency ratio for increasing Q^2 , as caused by propagation length effects (PL) and color transparency (CT).

the interaction cross section vanishes in the limit of large Q^2 . Then nuclear effects become negligible and color singlet transparency occurs.

The study of quark-gluon configurations of the interacting virtual photons requires a large lever-arm in Q^2 and ν . In addition one has to identify a kinematic window where the vector meson production process is most sensitive to coherent multiple scattering from several nucleons in the target nucleus. Finally, the influence of different characteristic scales on the production process have to be separated [19, 22, 23].

For these reasons coherent vector meson production from nuclei turns out to be very useful. At $|t| > 1/\langle r^2 \rangle_A$ the corresponding differential cross section depends crucially on contributions from coherent multiple scattering (Figure 2).

Coherent vector meson production is also favorable with respect to a separation of phenomena caused by variations of the propagation length and color transparency. This fact is demonstrated in Fig. 6: we compare the transparency ratio $\sigma_{\gamma^* A \rightarrow \rho A} / A \sigma_{\gamma^* N \rightarrow \rho N}$ for different values of Q^2 and ν as obtained within VMD. The decrease of the propagation length with rising Q^2 leads apparently to a suppression of the cross section ratio. If color transparency is fully established at large Q^2 only single scattering occurs. At large energies ν this leads to an increase of the transparency ratio as compared to the VMD

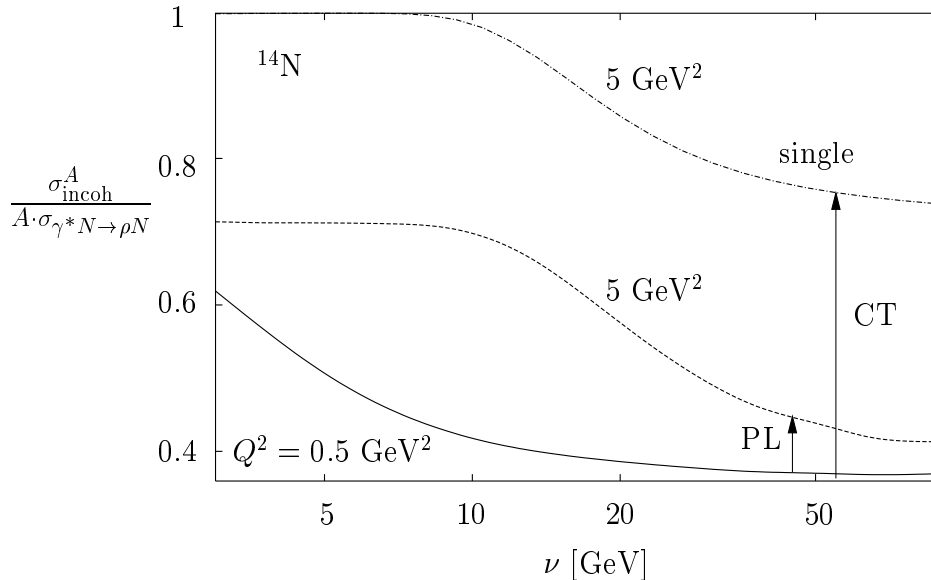


Figure 7: The transparency ratio for incoherent ρ production from ^{14}N . The full (dashed) curve corresponds to the VMD calculation at $Q^2 = 0.5 \text{ GeV}^2$ (5 GeV^2). The dash-dotted curve shows the single scattering result for $Q^2 = 5 \text{ GeV}^2$. The arrows indicate the behavior of the transparency ratio for increasing Q^2 , as caused by propagation length effects (PL) and color transparency (CT).

scenario. An increase of the transparency ratio with rising Q^2 is therefore a clear signal for the onset of color transparency.

In incoherent vector meson production the situation is different. As illustrated in Fig. 7, propagation length phenomena and color transparency lead to a similar trend for the Q^2 -dependence of the transparency ratio. A separation of both effects is therefore difficult. Similar observations have been made in [19].

The difference between both cases has two reasons. The first one is the reduction of the cross section by re-scattering contributions, a consequence of the fact that the scattering amplitudes are dominated by their imaginary parts. Therefore the color transparency effect which suppresses re-scattering always leads to a rise in the nuclear cross section relative to that of the free nucleon. On the other hand any changes in the propagation length affect primarily the coherent scattering process. Since $\sigma_{\text{incoh}}^A = \sigma_{\text{inclusive}}^A - \sigma_{\text{coh}}^A$, the coherent contribution enters with opposite sign when we consider incoherent scattering. This explains the difference between Fig. 6 and Fig. 7.

With the (simplistic) assumption that color transparency completely suppresses any re-scattering, its signature should be visible at $\nu = 50 \text{ GeV}$ when one systematically compares the range in Q^2 from 0.5 up to 5 GeV^2 , at least in our model. A more detailed calculation

requires in addition a model for the expansion of the initially small color dipole.

4 Summary

We have developed the multiple scattering formalism for the electroproduction of ρ mesons from nuclei. This process is an excellent tool to investigate the formation, propagation and hadronization of quark-antiquark-gluon fluctuations of the virtual high-energy photon.

The theory has been compared to the HERMES measurements for the case of ρ electroproduction on ^{14}N . The characteristic reduction of the nuclear transparency with increasing ρ meson propagation length is well reproduced. The more detailed quantitative analysis would still require an improved separation of incoherent and coherent events.

We have also examined the sensitivity with respect to the quest for color transparency in such processes. While the A -dependence of incoherent production does not permit a clear separation between color transparency and standard propagation length effects, coherent ρ electroproduction appears to be well suited for this purpose.

Acknowledgements

We would like to thank L. Frankfurt, M. Strikman, M. Sargsian, G. van der Steenhoven and T. O'Neill for discussions.

A Amplitudes and cross sections

A.1 Coherent amplitudes

We summarize the amplitudes for coherent ρ electroproduction used in our calculations up to $n = 2$. The simplifying assumption $\text{Re}f_\rho \ll \text{Im}f_\rho$ has been used.

$$f_{\gamma^*A \rightarrow \rho A}^{(0)}(\mathbf{k}_t) = AS_A(\mathbf{k}_t, -\Delta_{\gamma^*\rho})f_{\gamma^*\rho}(\mathbf{k}_t), \quad (33)$$

$$\begin{aligned} f_{\gamma^*A \rightarrow \rho A}^{(1)}(\mathbf{k}_t) = & i \frac{A(A-1)}{4\pi|\mathbf{q}|} \int d^2l f_\rho(\mathbf{k}_t/2 + \mathbf{l}) f_{\gamma^*\rho}(\mathbf{k}_t/2 - \mathbf{l}) \\ & \times S_A(\mathbf{k}_t/2 + \mathbf{l}, 0) S_A(\mathbf{k}_t/2 - \mathbf{l}, -\Delta_{\gamma^*\rho}), \end{aligned} \quad (34)$$

$$\begin{aligned} f_{\gamma^*A \rightarrow \rho A}^{(2)}(\mathbf{k}_t) = & - \frac{A(A-1)(A-2)}{32\pi^2|\mathbf{q}|^2} \int d^2l_1 \int d^2l_2 f_\rho(\mathbf{k}_t/3 + \mathbf{l}_1) \\ & \times f_\rho(\mathbf{k}_t/3 + \mathbf{l}_2) f_{\gamma^*\rho}(\mathbf{k}_t/3 - \mathbf{l}_1 - \mathbf{l}_2) \\ & \times S_A(\mathbf{k}_t/3 + \mathbf{l}_1, 0) S_A(\mathbf{k}_t/3 + \mathbf{l}_2, 0) S_A(\mathbf{k}_t/3 - \mathbf{l}_1 - \mathbf{l}_2, -\Delta_{\gamma^*\rho}). \end{aligned} \quad (35)$$

A.2 Inclusive cross sections

Here we give explicit expressions for the incoherent cross sections derived from the expansion of Eq.(11) for $n = 0, 1$. The $n = 0$ result reads:

$$\frac{d\sigma_{\gamma^*A \rightarrow \rho X}^{(0)}}{dt} = A \frac{d\sigma_{\gamma^*N \rightarrow \rho N}}{dt} [1 + (A-1)S_A(\mathbf{k}_t, -\Delta_{\gamma^*\rho})S_A(-\mathbf{k}_t, \Delta_{\gamma^*\rho})]. \quad (36)$$

The $n = 1$ result includes six additional interference terms between production and re-scattering amplitudes as well as the square of re-scattering amplitudes,

$$\frac{d\sigma_{\gamma^*A \rightarrow \rho X}^{(1)}}{dt} = \frac{d\sigma_{\gamma^*A \rightarrow \rho X}^{(0)}}{dt} + \sum_{i=1}^6 \left. \frac{d\sigma_{\gamma^*A \rightarrow \rho X}^{(1)}}{dt} \right|_i, \quad (37)$$

given by the following expressions:

$$\begin{aligned}
\left. \frac{d\sigma_{\gamma^*A \rightarrow \rho X}^{(1)}}{dt} \right|_1 &= -\frac{A(A-1)}{2|\mathbf{q}|^3} \int d^2l \operatorname{Im} [f_{\gamma^*\rho}^*(\mathbf{k}_t) f_{\gamma^*\rho}(\mathbf{k}_t - \mathbf{l}) f_\rho(\mathbf{l})] \\
&\times \{S_A(\mathbf{l}, 0)S_A(-\mathbf{l}, 0) + S_A(-\mathbf{k}_t + \mathbf{l}, \Delta_{\gamma^*\rho})S_A(\mathbf{k}_t - \mathbf{l}, -\Delta_{\gamma^*\rho}) \\
&\quad + (A-2)S_A(\mathbf{k}_t, -\Delta_{\gamma^*\rho})S_A(-\mathbf{k}_t + \mathbf{l}, \Delta_{\gamma^*\rho})S_A(-\mathbf{l}, 0)\},
\end{aligned} \tag{38}$$

$$\begin{aligned}
\left. \frac{d\sigma_{\gamma^*A \rightarrow \rho X}^{(1)}}{dt} \right|_2 &= \frac{A(A-1)}{8\pi|\mathbf{q}|^4} \int d^2l_1 \int d^2l_2 f_{\gamma^*\rho}^*(\mathbf{k}_t - \mathbf{l}_1) f_{\gamma^*\rho}(\mathbf{k}_t - \mathbf{l}_2) \\
&\times f_\rho^*(\mathbf{l}_1) f_\rho(\mathbf{l}_2) S_A(\mathbf{l}_1 - \mathbf{l}_2, 0) S_A(\mathbf{l}_2 - \mathbf{l}_1, 0),
\end{aligned} \tag{39}$$

$$\begin{aligned}
\left. \frac{d\sigma_{\gamma^*A \rightarrow \rho X}^{(1)}}{dt} \right|_3 &= \frac{A(A-1)(A-2)}{8\pi|\mathbf{q}|^4} \int d^2l_1 \int d^2l_2 f_{\gamma^*\rho}^*(\mathbf{k}_t - \mathbf{l}_1) f_{\gamma^*\rho}(\mathbf{k}_t - \mathbf{l}_2) \\
&\times f_\rho^*(\mathbf{l}_1) f_\rho(\mathbf{l}_2) S_A(\mathbf{l}_1 - \mathbf{l}_2, 0) S_A(-\mathbf{l}_1, 0) S_A(\mathbf{l}_2, 0),
\end{aligned} \tag{40}$$

$$\begin{aligned}
\left. \frac{d\sigma_{\gamma^*A \rightarrow \rho X}^{(1)}}{dt} \right|_4 &= \frac{A(A-1)(A-2)}{12\pi|\mathbf{q}|^4} \int d^2l_1 \int d^2l_2 f_{\gamma^*\rho}^*(\mathbf{k}_t - \mathbf{l}_1) f_{\gamma^*\rho}(\mathbf{k}_t - \mathbf{l}_2) \\
&\times f_\rho^*(\mathbf{l}_1) f_\rho(\mathbf{l}_2) S_A(-\mathbf{k}_t + \mathbf{l}_1, \Delta_{\gamma^*\rho}) S_A(\mathbf{k}_t - \mathbf{l}_2, -\Delta_{\gamma^*\rho}) S_A(\mathbf{l}_2 - \mathbf{l}_1),
\end{aligned} \tag{41}$$

$$\begin{aligned}
\left. \frac{d\sigma_{\gamma^*A \rightarrow \rho X}^{(1)}}{dt} \right|_5 &= \frac{A(A-1)(A-2)(A-3)}{16\pi|\mathbf{q}|^4} \\
&\times \int d^2l_1 \int d^2l_2 f_{\gamma^*\rho}^*(\mathbf{k}_t - \mathbf{l}_1) f_{\gamma^*\rho}(\mathbf{k}_t - \mathbf{l}_2) f_\rho^*(\mathbf{l}_1) f_\rho(\mathbf{l}_2) \\
&\times S_A(-\mathbf{k}_t + \mathbf{l}_1, \Delta_{\gamma^*\rho}) S_A(\mathbf{k}_t - \mathbf{l}_2, -\Delta_{\gamma^*\rho}) S_A(-\mathbf{l}_1, 0) S_A(\mathbf{l}_2, 0),
\end{aligned} \tag{42}$$

$$\begin{aligned}
\left. \frac{d\sigma_{\gamma^*A \rightarrow \rho X}^{(1)}}{dt} \right|_6 &= \frac{A(A-1)(A-2)}{24\pi|\mathbf{q}|^4} \\
&\times \int d^2l_1 \int d^2l_2 f_{\gamma^*\rho}^*(\mathbf{k}_t - \mathbf{l}_1) f_{\gamma^*\rho}(\mathbf{k}_t - \mathbf{l}_2) f_\rho^*(\mathbf{l}_1) f_\rho(\mathbf{l}_2) \\
&\times S_A(-\mathbf{k}_t + \mathbf{l}_1 - \mathbf{l}_2, \Delta_{\gamma^*\rho}) S_A(\mathbf{k}_t - \mathbf{l}_1, -\Delta_{\gamma^*\rho}) S_A(\mathbf{l}_2, 0).
\end{aligned} \tag{43}$$

The additional contributions to the $n = 2$ result, not shown here, are also included in the numerical calculations. They are constructed in exactly the same way as the expressions already shown by accounting for all possible combinations of struck nucleons.

References

- [1] HERMES, K. Ackerstaff et al., Phys. Rev. Lett. **82** (1999) 3025.
- [2] E665, M.R. Adams et al., Phys. Rev. Lett. **74** (1995) 1525.
- [3] NMC, M. Arneodo et al., Nucl. Phys. **B 429** (1994) 503.
- [4] V.N. Gribov, JETP **30** (1970) 709.
- [5] R.D. Spital and D.R. Yennie, Nucl. Phys. **106** (1976) 269 .
- [6] T.H. Bauer, R.D. Spital, D.R. Yennie and F.M. Pipkin, Rev. Mod. Phys. **50** (1978) 261.
- [7] S.J. Brodsky, L.L. Frankfurt, J.F. Gunion, A.H. Mueller and M.I. Strikman, Phys. Rev. **D 50** (1994) 3134.
- [8] F. Low, Phys. Rev. D **12**, 163 (1975); S. Nussinov, Phys. Rev. Lett. **34**, 1286 (1975); J. F. Gunion and D. Soper, Phys. Rev. D **15**, 2617 (1977)
- [9] S.J. Brodsky and A.H. Mueller, Phys. Lett. **B 206** (1988) 685.
- [10] N.N. Nikolaev, Comments Nucl. Part. Phys. **21** (1992) 41.
- [11] L.L. Frankfurt, G.A. Miller and M. Strikman, Ann. Rev. Nucl. Part. Sci. **44** (1994) 501.
- [12] P. Jain, B. Pire and J.P. Ralston, Phys. Reports **271** (1996) 67.
- [13] G. Piller and W. Weise, Phys. Reports **330** (2000) 1.
- [14] L.L. Frankfurt, W. Koepf and M.I. Strikman, Phys. Rev. **D 54** (1996) 3194.
- [15] D. R. Yennie, in *Hadronic Interactions of Electrons and Photons*, edited by J. Cummings and D. Osborn, **321** (1971).
- [16] W. Czyz and L.C. Maximon, Ann. of Physics **52** (1969) 59.
- [17] H. Fraas and D. Schildknecht, Nucl. Phys. **B 14** (1969) 543.
- [18] J.A. Crittenden, Springer, Tracts in Modern Physics **140** (1997).
- [19] B.Z. Kopeliovich and J. Nemchik, preprint MPIH-V41-1995, nucl-th/9511018.
- [20] J. Hüfner, B.Z. Kopeliovich and J. Nemchik, Phys. Lett. **B 383** (1996) 362.
- [21] H. De Vries, C.W. de Jager and C. De Vries, Atomic Data and Nuclear Data Tables **36** (1987) 495.
- [22] L.L. Frankfurt, W. Koepf, J. Mutzbauer, G. Piller, M. Sargsian, M.I. Strikman, Nucl. Phys. **A 622** (1997) 511.
- [23] L.L. Frankfurt, G. Piller, M. Sargsian, M.I. Strikman, Eur. Phys. J. **A 2** (1998) 301.

- [24] M.R. Adams et al., E665 Collaboration, *Z. Phys.* **C74** (1997) 237.
- [25] The New Muon Collaboration, *Nucl. Phys.* **B 429** (1994) 503.
- [26] S. Aid et al., H1 Collaboration, *Nucl. Phys.* **463** (1996) 3.
- [27] S. Aid et al., H1 Collaboration, *Nucl. Phys.* **468** (1996) 3.
- [28] J. Breitweg et al., ZEUS Collaboration, *Z. Phys.* **C2** (1998) 247.
- [29] ZEUS Collaboration, DESY 98-107, (1998).
- [30] W.D. Shambroom et al., CHIO Collaboration, *Phys. Rev.* **D 26** (1982) 1.